Influence of Micro Sandblasting on the Surface Integrity of the AlTiN Coated Tool Material

Zhou Yu
School of Mechanical Engineering, Shandong University of Technology, 266 West Xincun Road, Zibo 255000, China

Yujuan Dong
3College of Preschool Education, Zibo Normal College, 99 Tangjun Ouling Road, Zibo 255130, China

Guangming Zheng (zhengguangming@sdut.edu.cn)
School of Mechanical Engineering, Shandong University of Technology, 266 West Xincun Road, Zibo 255000, China

Xiuli Jiang
Shandong Provincial Institute of Mechanical Design, 129 Jiluo Rode, Jinan 250031, China

Xiang Cheng
School of Mechanical Engineering, Shandong University of Technology, 266 West Xincun Road, Zibo 255000, China

Xianhai Yang
School of Mechanical Engineering, Shandong University of Technology, 266 West Xincun Road, Zibo 255000, China

Kaishuo Chang
School of Mechanical Engineering, Shandong University of Technology, 266 West Xincun Road, Zibo 255000, China

Xuewei Li
School of Mechanical Engineering, Shandong University of Technology, 266 West Xincun Road, Zibo 255000, China

Research Article

Keywords: Micro sandblasting, Surface integrity, Coated tool, Flow field, Residual stress

Posted Date: July 28th, 2021

DOI: https://doi.org/10.21203/rs.3.rs-746083/v1

Abstract

Due to the high-efficiency, environmental protection the low cost, the micro sandblasting technology is used in the surface treatment of the coated tools. The simulation and application of micro sandblasting of the coated tool are carried out to reveal the surface treatment mechanism and analyze the influence of sandblasting parameters on the tool surface integrity. The flow field erosion simulation model of abrasive-water-air three-phase flow is established. The results show that the maximum velocity and pressure are obtained at the center of jet flow. The pressure distribution on the target surface has little correlation with the distance to the nozzle. The surface morphology of the AlTiN coated tool changes obviously after micro sandblasting. Moreover, the low surface roughness R_a of the blasted tool can be obtained at the small sandblasting pressure and time. Additionally, the residual compressive stress on the surface of the AlTiN coated tool is enhanced after micro sandblasting. This work has practical significance for optimizing micro sandblasting process and improving the surface integrity of coated tools.

1 Introduction

With the development of the modern manufacturing industry, the demand for reworking metal workpiece is increasing. Cutting tools play an important role in it, especially in hard to machine materials. The tool wear is particularly prominent. And the renewal frequency of new tool is increased. So, the cutting cost is increased [1]. To solve such problems, most factories use coated tools. The service life of the coated tool is longer than that of the ordinary tool. And the surface quality is improved effectively. But the coated tool of better quality is more expensive. Due to the significant performance improvement, high-efficiency, low cost and other advantages, the surface treatment technology is used in the cutting tools. At present, more commonly used surface treatment technologies are laser treatment, mechanical polishing, mechanical treatment, heat treatment and so on [2–5]. As one of the surface treatment technologies, the micro sandblasting has been widely used in the surface treatment of coated tools, because of its advantages of simple operation, high-efficiency, safety and pollution-free, high improvement of cutting performance.

Micro sandblasting is an unconventional subtractive micro-manufacturing technology, which is developed from abrasive jet machining. As an efficient and environmentally surface treatment technology, it has attracted extensive attention in recent years. It is reported that the micro sandblasting process is suitable for treating of some small size workpiece [6], especially for the surface treatment of coated tool. In the wet-type micro sandblasting process, the high-pressure gas is used to push the mixture of abrasive and water to hit the coated tool surface. The size of abrasive is usually measured in microns (5-100μm). The commonly used abrasive materials mainly include Al_2O_3, AlSi, ZrO_2, SiO_2, etc. The sandblasting pressure range is 0.1–0.5 MPa, and the time range is 1–10 s [7]. The impact strengthening effect of abrasive material can strengthen the cohesive strength between coating and substrate.

Micro sandblasting has an important influence on the surface properties, cutting performance and wear resistance of coated tools. The effect of micro sandblasting on the coated cemented carbide tool is

investigated [8]. The influences of abrasive particles (Al_2O_3 and ZnO_2) on the hardness and brittleness of coated carbide inserts, tool geometry, and tool life are investigated. They found that micro sandblasting can improve the cutting performance of coated tools. Additionally, micro-sandblasting could increase the compressive stress of the coating surface [9]. At the same time, the hardness and brittleness of coating are improved. It is proposed that the micro sandblasting could not only improve the tool wear and cutting performance, but also improve the tribological performance and adhesion of the coating [10]. During high-speed milling of AISI 4140 (42CrMo4) steel with treated carbide tool, it is found that the micro sandblasting can improve the fracture resistance of the carbide tool [11]. The micro-sandblasting is used to treat the CrN coated samples [12]. It is found that the micro-sandblasting process does not have a negative effect on the hardness, adhesion strength and fatigue resistance of the coated samples. The effect of dry micro sandblasting on the fracture resistance of the PVD-AlTiN coated carbide cutting tools is also studied [13]. The results show that micro sandblasting surface treatment technology can prevent the coating lamination and improve the wear resistance. Other researchers also found that micro-sandblasting can improve the life of coated tools [14]. Compared with the commercial tools on the market today, the tool life obtained in its research is three times longer [14]. Compared with the coated tool without any treatment, the hardness of the AlTiN coating is increased after micro sandblasting [7]. According to the appropriate wet micro sandblasting process parameters, CVD coated tools with good wear resistance can be prepared [15]. The effect of sandblasting on the tribological properties of TiN/ MT-TiCN /Al_2O_3/TiCNO coating is investigated [16]. The micro sandblasting can improve the adhesion of the coating and reduce the appearance of microcracks on the coating surface. It is pointed that the micro sandblasting plays an important role in improving the wear resistance of coating [16]. It is also addressed that micro sandblasting can improve the wear resistance of TiN coating [17]. Additionally, the micro sandblasting can also improve the residual compressive stress, reduce the production of microcracks, and increase the fatigue life of the tool [18–20].

The micro sandblasting process is a complex process that the mixture of abrasive and water reaches the tool surface through an air medium [21]. It is difficult to observe the distribution state of the jet in the flow field and analyze the stress change of the treated surface effectively. With the development of computational fluid dynamics, the complex motion of incompressible fluid can be simulated by using technical software [22]. In this work, FLUENT simulation software is used to simulate the process of high-pressure jet impinging on the tool surface. At the same time, the simulation process is verified by micro sandblasting test. The changes in surface morphology and physical properties of the blasted coated tool are studied. The research is helpful to set the parameters of tool surface treatment and improve machining efficiency. It can provide some technical reference and guidance for tool post-processing.

2 Material And Methods

2.1 Jet structure model

Figure 1a shows the schematic diagram of micro-abrasive water jet. The high-pressure gas pushes the mixture of abrasive and water through the Venturi into the nozzle. And then, the micro-abrasive water jet enters the flow field from the nozzle to reach the target surface. This process is divided into three stages: initial stage, basic stage and dissipative stage. In the initial stage, the jet leaves the nozzle and enters the flow field area. The jet formed by abrasive and water have exchange energy with the air medium. The jet flow at the nozzle is in a tight convergence state. At this point, the maximum of the velocity and pressure is obtained at the center of jet flow. With the increase of axial distance (away from the nozzle), the pressure and velocity show a downward trend. In the basic stage, the jet kinetic energy is further consumed. The radial section pressure of jet decreases gradually from the center to the outside. With the increase of axial distance, the velocity and radial pressure continue to show a downward trend, which is similar to hyperbola. In the dissipation stage, a large amount of air is mixed in the jet and distributed as mist. At this time, the jet pressure and velocity are minimal. The energy exchange between the jet and the environment reaches a balanced state.

2.2 3D model of flow field

As shown in Fig. 1b, the pre-processing software ICEM under ANSYS is used. The three-dimensional model of simulated flow field is established and meshed. After the boundary condition encryption, 942213 grids are divided. The grid quality is above 0.355. The high-quality grid can meet the requirements of flow field simulation operation.

The nozzle adopts pressure inlet boundary condition. The pressure of outlet is one standard atmosphere. The Eulerian model is selected for the multiphase flow model. The solver selection is based on the pressure solver. The SIMPLE pressure velocity coupling method is adopted. The simulation phase is provided with three phases, namely gas, liquid, and solid. The solid phase is Al_2O_3 or ZrO_2. Water is the main phase. The turbulence model is standard K-Epsilon. The target surface is 300 mm away from the nozzle exit.

The basic process of simulation is as follows. The high-pressure jet formed by solid particles and water enters the flow field through the nozzle. Then, the jet impinges on the target surface through the air medium through the flow field. The impact of the abrasive material on the tool surface during micro sandblasting is simulated.

2.3 Micro sandblasting experiment

The tools selected are carbide coated inserts produced by Kennametal Company. The coating material is AlTiN and the brand is KC522M. The specific parameters of the abrasive materials are shown in Table 1. A wet-type micro sandblasting machine is used in the test. The type of micro sandblasting is 9080-2W-ZSK(China). The experimental design of wet micro sandblasting process is shown in Fig. 2. The micro sandblasting machine is mainly composed of a sandblasting room, control panel, gun assembly, workpiece fixture, pressure regulating system, and so on. The blasting angle shall be 90° (vertical injection). The sandblasting method is automatic sandblasting. The installation and clamping mode of the insert is shown in Fig. 2b.

Table 1
Specific parameters of the abrasive materials.

Parameter	Al_2O_3	ZrO_2
Particle size	26μm	26μm
Geometrical shape	polygonal	globular
Vickers hardness (HV)	2400	1300
Density ($g.cm^{-3}$)	3.6	5.89
Elastic modulus (GPa)	420	300
Yield strength (GPa)	4.8	4
Ultimate strength (GPa)	7	6

Single factor method is adopted to carry out the test. Three test factors are selected with the following parameters: abrasive type of Al_2O_3 and ZrO_2, sandblasting pressure p = 0, 0.1, 0.3, 0.5 MPa, sandblasting time t = 1, 3, 5, 7 s.

2.4 Test methods

After micro sandblasting, a variety of instruments are used to detect the treated tool. Firstly, ultrasonic cleaning instrument is used to clean the treated tool. Then, Quanta250 scanning electron microscope (SEM) is used to observe the surface morphology of the treated tool. An optical profiler (model: WYKO NT9300, Germany) is used to measure the surface roughness R_a. In this work, the surface roughness R_a is taken as the average value of five measurements. In addition, X-ray stress analyzer (model: X-3000, Finland) is used to detect the tool surface residual stress. The measured average value of residual stress is selected in the work.

3 Results And Discussion

3.1 Flow field erosion simulation analysis

3.1.1 Pressure and velocity *of flow field*

Figure 3 shows the pressure cloud map and velocity cloud diagram of the flow field at pressure of 0.3 MPa with Al_2O_3 solid phase. As can be seen in Fig. 3a, the water flow enters the flow field from the pressure inlet. When the jet enters the nozzle. The pressure increases sharply due to the contraction of the inner diameter of the pipe. At the nozzle outlet pressure reaches the maximum value and tends to be stable. When the jet enters the external flow field (standard atmospheric pressure). The maximum of the jet pressure in the axial direction. And the pressure distribution spreads out in a "trumpet" shape. As can be seen in Fig. 3b, the velocity reaches its maximum at the jet axis and the jet velocity presents a

scattering state. When the jet enters the external field, the kinetic energy of the jet is gradually affected by air resistance. So, the velocity distribution decreases in the axial and radial direction. When the efflux reaches the target surface through the external flow field, the jet has been blocked by the target surface. So, the minimum of velocity is in the direction of axial and diameter.

Figure 4 shows the variation of pressure and velocity along x axial coordinate, from which can be seen that the same drop law of the jet in the flow field is displayed at different pressures. With the increase of axial distance, the pressure presents a trend of decrease (Fig. 4a). When the jet enters the flow field, it will exchange energy and potential energy with air. The longer the distance from the nozzle, the longer the conversion time between potential energy, and the lower the pressure at the axis. At any position in the flow field, however, the jet pressure at the axis always keeps at the maximum value of the radial interface (Fig. 3a). As can be seen in Fig. 4b, the velocity at the nozzle is 26 m/s, 23 m/s and 12.5 m/s when the jet pressure is 0.5 MPa, 0.3 MPa and 0.1MPa, respectively. With the increase of x axial distance, the velocity tends to decrease. The velocity decreases sharply when the jet comes into contact with the target surface. When the jet enters the flow field area, the velocity reaches its maximum. With the increase of x axial distance, the kinetic energy gradually exchanges energy with air. And the velocity gradually decreases. When the mixture of abrasive and water hits the target surface, the kinetic energy is converted into potential energy. Thus, the velocity decreases sharply.

To sum up, with the increase of the distance from the nozzle, the jet pressure and velocity all show a downward trend. However, the high pressure of the jet does not indicate the enhancement of the tool surface performance. So the specific parameter setting needs to be adjusted flexibly according to the actual situation.

3.1.2 Pressure and stress of target surface

Figure 5 shows the pressure cloud map of target surface (x = 300 mm), from which can be seen that the closer to the center of the target surface, the greater the pressure is. The pressure away from the center gradually decreases until it disappears. The pressure cloud map presents a symmetric distribution of the center. Although sandblasting pressures are different, the same distribution is presented on the target surface. By contrast, the higher the sandblasting pressure is, the more concentrated the jets are. Because of the scattering of the jet beam, the area of the center circle is larger when the jet impinges on the target surface. Therefore, the pressure on the target surface decreases with the reduce of sandblasting pressure. The jet beam scatters and the target pressure decrease from the center to the edge until it disappears.

Figure 6 shows the shear stress cloud map of target surface (x = 300 mm). The shear stress near the center of the target surface is obvious. And the shear stress around the center area is greater than that at the center point. The farther it is from the center of the target plane, the shear stress decreases and disappears. In the actual sandblasting process, the micro-abrasive jet generates shear stress on the target surface. It can not only remove impurity particles on the tool surface, but also improve the surface roughness.

Figure 7 shows the variation of pressure and shear stress along *y* axial coordinate. As can be seen from Fig. 7a, the highest pressure is obtained at the center of target surface. The pressure at the edge of the target is the lowest and approaches zero. The pressure of jet impinging on the target surface is similar at different sandblasting pressures. The pressure is distributed symmetrically from the center to the edge of the target surface. And the pressure curve presents Gaussian normal distribution curve. With the increase of sandblasting pressure, the pressure on the center of the target surface is higher. So, it is suggested that the coated tool should be put in the center of the jet to avoid uneven pressure when jet impinges on tool surface in the sandblasting process. As can be seen from Fig. 7b, the similar shear stress distribution is presented at different sandblasting pressure, showing a similar "hump" downward trend. The maximum shear stress is not located at the center of the target plane. In a small area around the center of the target plane, the shear stress roughly presents the distribution of the high edge bottom of the center, which is different from the distribution of the stress on the target plane.

Figure 8 shows the spray distribution cloud map at $x = 100$ mm and $x = 300$ mm. It can be observed that the distribution state of the spray near the nozzle is also symmetrical in the center at $x = 100$ mm (Fig. 8a). Because the jets are relatively concentrated, the injected material is not completely distributed $x = 100$ mm. The area near the center produces a partial cavity. The reason is that the central area of the injected material is faster and some of the air is mixed in it. As can be seen from Fig. 8b, the spraying material covers the entire target surface at $x = 300$ mm. When the spray material reaches the target surface, the abrasives exchange energy with air. The kinetic energy of the spraying material is reduced. And the spraying material impacts the target surface in the form of fog. The further away from the nozzle, the greater area of spray on the target surface is. The distribution area of the spray decreases with the increase of radial distance. In the actual process of micro sandblasting. The blasting distance should be controlled reasonably. If it is too close to the nozzle, it causes uneven sandblasting on the tool surface. And there is no sandblasting effect at the edge of the tool. If it is too far from the nozzle, the pressure of the injection material on the tool surface will be too small. This is not be able to get the effect of micro sandblasting.

According to the simulation analysis of the pressure and velocity flow field, the shear stress and pressure of target surface. It

The flow field erosion model can indirectly simulate the impact of jet on the tool surface in the process of micro sandblasting. Reasonable prediction and analysis are made on the influence of the tool surface. It can provide a reference for the parameter design of micro sandblasting.

3.2 Surface integrity of the coated tool

3.2.1 Surface morphology

Figure 9 shows the effect of abrasive on surface morphology of coated tool at $t = 5$ s and $p = 0.3$ MPa. As shown in Fig. 9a, the coating surface is treated by ZrO_2 abrasive. The jet is composed of abrasive and water impinges on the coated tool surface under the push of high-pressure gas. The shear stress

generated by the jet removes impurity particles from the coating surface. The white areas are tiny pits left by the impact of the ZrO_2 abrasive (Fig. 9a). As shown in Fig. 9b, the area of white area and the pits on the tool surface are increased, which is caused by the difference in the shape of the abrasive itself. ZrO_2 injection material is spherical structure, while Al_2O_3 is irregular polygonal. When an irregular prism strikes the surface of the coating, the shape of the abrasive itself will break again, which produce more sharp abrasive. Thus, the sandblasting effect on the coating surface is enhanced. It also leads to an increase in surface roughness. Therefore, Al_2O_3 is more erosive to coatings, which also has a higher removal rate of the coating.

Figure 10 shows the effect of sandblasting pressure and time on surface morphology of coated tool with abrasive of Al_2O_3. At $t = 3$ s, the tiny pits (white areas) appear on the coating surface (Fig. 10b). This is the mark left by the abrasive material hitting the surface of the coating. At $t = 5$ s, the coating coverage of the tool base layer decreases obviously (Fig. 10c). Parts of the tool substrate are exposed. At $t > 7$ s, the blasting particles impact the coating for a long time. The coating disappears completely and parts of the tool substrate are exposed (Fig. 10d). Therefore, the extension of sandblasting blasting time can cause part of the tool coating to fall off. Then, the tool performance will degrade. At the same time, the thermal protection performance of the coated tool also disappears. During cutting process, the abrasion degree of the tool increases and the tool life decreases. At $p = 0.1$ MPa, the particle morphology of the coated tool surface significantly disappears and the surface becomes smoother (Fig. 10e). When the sandblasting pressure increases to 0.5 MPa (Fig. 10f), the impact of abrasive increases the shedding area of coating. Some parts of the tool substrate leak out. The thermal barrier function of the coating is destroyed, and coating surface defects are correspondingly increased. Just as the simulation results, the higher sandblasting pressure can give a strong impact pressure on the tool surface (Figs. 5 and 7). And the shear stress on the tool surface by jet flow is also large (Figs. 6 and 7). If the sandblasting pressure is too low, the impurity particles on the tool surface cannot be removed. It will not have any effect on the tool surface. However, the excessive sandblasting pressure can lead to a strong jet flow, which can produce a large shear stress. It not only affects the cutting performance of the tool, but also reduces its service life.

Therefore, the even surface morphology of the treated coated tool can be obtained at sandblasting pressure $p = 0.1 \sim 0.3$ MPa and sandblasting time $t = 3 \sim 5$ s.

3.2.2 Surface roughness

Figure 11 shows the effect of sandblasting parameters on surface roughness R_a. Under the same micro sandblasting condition, the surface roughness R_a of the coated tool after sandblasting by Al_2O_3 abrasive is 0.423 μm (Fig. 11a), which is higher than that of the untreated tool. On the other hand, after ZrO_2 micro sandblasting, the surface roughness R_a is 0.187 μm, which is lower than that of the untreated tool. It is verified that Al_2O_3 abrasive has a stronger impact on the coating.

As can be seen from Fig. 11b, with the increase of sandblasting pressure, the surface roughness R_a presents a rising trend. The initial surface roughness R_a is 0.236 μm. As the sandblast pressure increases,

the impact force of the abrasive against the tool surface is improved. When the abrasive hits the tool surface, the solid impurities will be removed from the tool surface. However, the sharp edges and corners of Al_2O_3 itself can damage the coating surface. Part of the coating is detached from the tool substrate. This results in a larger value of the surface roughness R_a. When the sandblasting pressure is 0.5 MPa, the surface roughness R_a is 0.528 μm. The reason for the increase of surface roughness R_a is the falling off of coating. Therefore, a suitable pressure range can avoid the erosion of coating.

As shown in Fig. 11c, the minimum surface roughness R_a is obtained at t = 1 s with the abrasive material of Al_2O_3, while the minimum surface roughness R_a is obtained at t = 7 s with the abrasive material of ZrO_2. The sharp part of Al_2O_3 abrasive causes the impurity particles on the coating surface to be removed first at t = 1 s. so the surface roughness is reduced. At t = 3 s, the Al_2O_3 abrasive hitting the coating surface will produce large pits, increasing surface roughness. When the sandblasting time exceeds 3 s, the coating removal rate and the shallow surface pits are enhanced and the. Therefore, the surface roughness R_a is decreased, and the coating surface becomes smoother. On the other hand, with the extension of sandblasting time, the surface roughness R_a shows a decreasing trend when ZrO_2 abrasive is used. Only small pits are induced by ZrO_2 abrasive. The deposition particles and defects on the coating surface are eliminated. The surface becomes smoother and the surface roughness is R_a decreased.

Therefore, the high surface roughness R_a can be contributed by Al_2O_3 abrasive at high sandblasting pressure and long sandblasting time.

3.2.3 Surface residual stress

In the process of micro sandblasting, the jet composed of abrasive and water continuously impinges on the tool surface. The previous simulation results show that the high-pressure jet will have a strong impact force on the tool surface. The residual stress level on the coated tool surface is enhanced accordingly.

Figure 12 shows the effect of sandblasting parameters on residual stress, from which can be seen that the level of residual compressive stress is further improved after sandblasting. As can be seen in Fig. 12a, the residual stress on the tool surface treated by Al_2O_3 is -864 MPa, increasing by about 29.5% compared with that of the untreated tool. After ZrO_2 treatment, the tool surface residual stress is -748 MPa, which is increased by 12.1%. During high-speed cutting process, the higher residual compressive stress can inhibit the formation of microcracks on the tool surface. Thus, the cutting performance of the tool can be improved.

As can be seen in Fig. 12b, with the increase of sandblasting pressure, the compressive stress (absolute value) presents a trend of first increasing and then decreasing. The impact of jet beam is not only conducive to the removal of impurity particles on the tool surface, but also can increase the residual stress on the tool surface. The greater the jet pressure is, the greater the impact strength on the tool surface will be. So, the highest residual stress (absolute value) is obtained at p = 0.3 MPa. Once the sandblasting pressure exceeds 0.3 MPa. The strong jet pressure accompanied by the spray particles can

remove part of the tool coating material. The reduction of coating thickness can cause part of the coating to fall off from the tool substrate. Thus, the surface residual compressive stress (absolute value) is reduced at $p = 0.5$ MPa.

As can be seen in Fig. 12c, with the extension of sandblasting time, the residual compressive stress (absolute value) on the tool surface is enhanced. The abrasive particles are constantly bumping into the coating surface. The impact on the tool surface is stronger due to the Al_2O_3 abrasive with sharp shape. The surface residual compressive stress (absolute value) is significantly increased.

To sum up, the high level of surface integrity (e.g. low surface roughness R_a, even surface morphology and high residual compressive stress (absolute value)) for the AlTiN coated tool can result from sandblasting pressure $p = 0.1 \sim 0.3$ MPa and sandblasting time $t = 3–5$ s with Al_2O_3 abrasive.

4 Conclusion

The flow field erosion model is established to simulate the coated tool for micro sandblasting in the early stage, and the effective analysis is carried out in the later stage through experiments. From the present work, the following conclusions are drawn.

1. When the jet enters the external flow field (standard atmospheric pressure), the maximum of the velocity and pressure is obtained at the center of jet flow. The pressure and the shear stress on the target surface are decreased from the center to edge until it disappears. The shear stress around the center area of the target surface is larger than the shear stress at the center point.
2. With it the extension of micro sandblasting time, the deposition particles and defects on the coating surface are eliminated. And the surface roughness R_a is reduced. Under the same sandblasting parameters, the residual compressive stress on the tool surface is increased to a higher level when Al_2O_3 abrasive is used.
3. For the AlTiN coated tool, the high level of surface integrity can be caused by Al_2O_3 abrasive at $p = 0.1 \sim 0.3$ MPa and $t = 3–5$ s.

Declarations

Acknowledgments

This work was supported by the Natural Science Foundation of Shandong Province [No. ZR2020ME156, ZR2020ME157], National Key Research and Development Program of China [No. 2018YFB2001400], and the National Natural Science Foundation of China [No. 52075306].

Author contribution

Zhou Yu: Conceptualization, Methodology, Formal analysis, Investigation, Writing -Original Draft, Writing - Review & Editing. Yujuan Dong: Methodology, Writing - Review & Editing. Guangming Zheng:

Investigation, Formal analysis, Writing - Review & Editing, Supervision. Xiuli Jiang: Writing - Review & Editing. Xiang Cheng: Methodology, Formal analysis. Xianhai Yang: Methodology, Investigation, Formal analysis. Kaishuo Chang: Writing - Review & Editing. Xuewei Li: Methodology, Formal analysis.

Ethics approval: Not applicable

Consent to participate: Not applicable

Consent for publication: The copyright permission has been taken, and consent to submit has been received explicitly from all authors.

Competing interests: The authors declare no competing interests.

References

[1] S. Azim, S. Gangopadhyay, S.S. Mahapatra, R. Mittal, R.K. Singh, Role of PVD coating on wear and surface integrity during environment-friendly micro-drilling of Ni-based superalloy, Journal of Cleaner Production 272 (2020) 122741, https://doi.org/10.1016/j.jclepro.2020.122741.

[2] M.S. Zoei, M.H. Sadeghi, M. Salehi, Effect of grinding parameters on the wear resistance and residual stress of HVOF-deposited WC-10Co-4Cr coating, Surface & Coatings Technology 307 (2016) 886-891, https://doi.org/10.1016/j.surfcoat.2016.09.067

[3] K.-D. Bouzakis, P. Charalampous, T. Kotsanis, G. Skordaris, E. Bouzakis, B. Denkena, B. Breidenstein, J.C. Aurich, M. Zimmermann, T. Herrmann, R. M'saoubi, Effect of HM substrates' cutting edge roundness manufactured by laser machining and micro-blasting on the coated tools' cutting performance, CIRP Journal of Manufacturing Science and Technology 18 (2017) 188-197, https://doi.org/10.1016/j.cirpj.2017.02.003.

[4] E.E. Yunata, T. Aizawa, K. Tamaoki, M. Kasugi, Plasma polishing and finishing of cvd-diamond coated WC (Co) dies for dry stamping, Procedia Engineering 207 (2017) 2197-2202, https://doi.org/10.1016/j.proeng.2017.10.981.

[5] Y. Qin, H. Zhao, C. Li, J. Lu, J. He, Effect of heat treatment on the microstructure and corrosion behaviors of reactive plasma sprayed TiCN coatings, Surface and Coatings Technology 398 (2020) 126086, https://doi.org/10.1016/j.surfcoat.2020.126086.

[6] R. Giti, S. Haghdoost, E. Ansarifard, Effect of different coloring techniques and surface treatment methods on the surface roughness of monolithic zirconia, Dental Research Journal 17 (2020) 152-161, https://doi.org/10.4103/1735-3327.280893.

[7] A. Jacoba, S. Gangopadhyay, A. Satapathy, S.Mantry, B.B. Jhab.. "Influences of micro sandblasting as surface treatment technique on properties and performance of the AlTiN coated tools, Journal of Manufacturing Processes 29 (2017) 407-418, https://doi.org/10.1016/j.jmapro.2017.08.013.

[8] K.-D. Bouzakis, F. Klocke, G. Skordaris, E. Bouzakis, S. Gerardis, G. Katirtzoglou, S. Makrimallakis, Influence of dry micro-blasting grain quality on wear behaviour of TiAlN coated tools, Wear 271 (2011) 783-791, https://doi.org/10.1016/j.wear.2011.03.010.

[9] K.-D. Bouzakis, G. Skordaris, E. Bouzakis, A. Tsouknidas, S. Makrimallakis, S. Gerardis, G. Katirtzoglou, Optimization of wet micro-blasting on PVD films with various grain materials for improving the coated tools' cutting performance, CIRP Annals - Manufacturing Technology 60 (2011) 587-590, https://doi.org/10.1016/j.cirp.2011.03.012.

[10] S.B. Abusuilik, K. Inoue, Effects of intermediate surface treatments on corrosion resistance of cathodic arc PVD hard coatings, Surface and Coatings Technology 237 (2013) 421-428, https://doi.org/10.1016/j.surfcoat.2013.09.026.

[11] S.B. Abusuilik, Pre-, intermediate, and post-treatment of hard coatings to improve their performance for forming and cutting tools, Surface and Coatings Technology 284 (2015) 384-395, https://doi.org/10.1016/j.surfcoat.2015.07.003.

[12] C. Petrogalli, L. Montesano, A. Pola, M. Gelfi, A. Ghidini, G.M. LaVecchiaa, Improvement of Fatigue Resistance of a Tool Steel by Surface Treatments, Procedia Engineering 109 (2015) 154-161, https://doi.org/10.1016/j.proeng.2015.06.227.

[13] S. Tanaka, T. Shirochi, H. Nishizawa, K. Metoki, H. Miura, H. Hara, T. Takahashi, Micro-blasting effect on fracture resistance of PVD-AlTiN coated cemented carbide cutting tools, Surface and Coatings Technology 308 (2016) 337-340, https://doi.org/10.1016/j.surfcoat.2016.07.094.

[14] C. Puneet, K. Valleti, A.V. Gopal, Influence of surface preparation on the tool life of cathodic arc PVD coated twist drills, Journal of Manufacturing Processes 27 (2017) 233-240, https://doi.org/10.1016/j.jmapro.2017.05.011.

[15] C. Liu, Z. Liu, B. Wang, Modification of surface morphology to enhance tribological properties for CVD coated cutting tools through wet micro blasting post-process, Ceramics International 44 (2018) 3430-3439, https://doi.org/10.1016/j.ceramint.2017.11.142.

[16] T. Shen, L. Zhu, Z. Liu, Effect of micro-blasting on the tribological properties of TiN/MT-TiCN/Al_2O_3/TiCNO coatings deposited by CVD, International Journal of Refractory Metals and Hard Materials 88 (2020) 105205, https://doi.org/10.1016/j.ijrmhm.2020.105205.

[17] R. Mundotia, D.C. Kothari, A. Kale, U. Mhatre, K. Date, N. Thorat, T. Ghorudea, Effect of ion bombardment and micro sandblasting on the wear resistance properties of hard TiN coatings, Materials Today: Proceedings 26 (2020) 603-612, https://doi.org/10.1016/j.matpr.2019.12.171.

[18] L. Faksa, W. Daves, W. Ecker, T. Klünsner, M. Tkadletz, C. Czettl, Effect of shot peening on residual stresses and crack closure in CVD coated hard metal cutting inserts, International Journal of Refractory

Metals and Hard Materials 82 (2019) 174-182, https://doi.org/10.1016/j.ijrmhm.2019.04.008.

[19] D.P. Gruber, D. Kiefer, R. Rössler, F. Beckmann, M. Tkadletz, T. Klünsner, C. Czettl, J. Keckes, and J. Gibmeier, 20 Hz synchrotron X-ray diffraction analysis in laser-pulsed WC-Co hard metal reveals oscillatory stresses and reversible composite plastificationm, International Journal of Refractory Metals and Hard Materials, 82 (2019) 121-128. https://doi.org/10.1016/j.ijrmhm.2019.04.004.

[20] Thakur, R.K., and K.K. Singh, Experimental investigation and optimization of abrasive water jet machining parameter on multi-walled carbon nanotube doped epoxy/carbon laminate, Measurement 164 (2020) 108093 https://doi.org/10.1016/j.measurement.2020.108093.

[21] Bouzakis, K.-D., S. Makrimallakis, G. Katirtzoglou, G. Skordaris, S. Gerardis, E. Bouzakis, T. Leyendecker, S. Bolz, and W. Koelkerc, Adaption of graded Cr/CrN-interlayer thickness to cemented carbide substrates' roughness for improving the adhesion of HPPMS PVD films and the cutting performance, Surface and Coatings Technology 205 (2010) 1564–1570. https://doi.org/10.1016/j.surfcoat.2010.09.010.

[22] R. Melentiev, F. Fang, Investigation of erosion temperature in micro-blasting, Wear 420-421 (2019) 123-132. https://doi.org/10.1016/j.wear.2018.12.073.

Figures

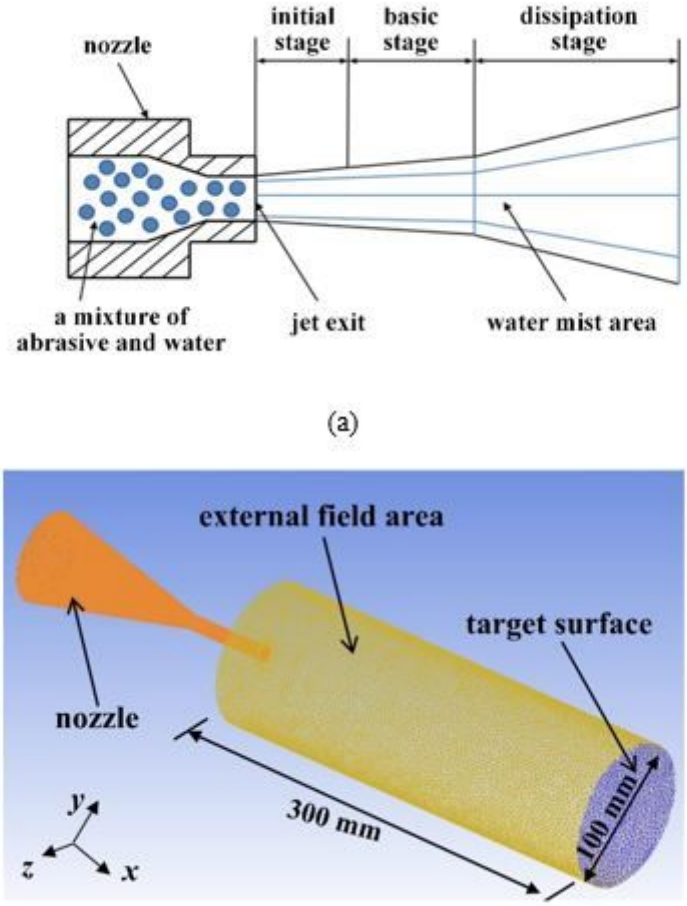

Figure 1

Schematic diagram of (a) micro-abrasive water jet and (b) flow field simulation grid division.

(a)

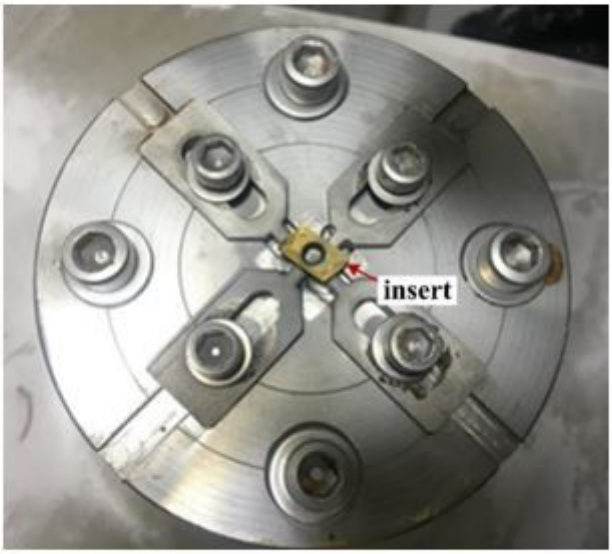

(b)

Figure 2

Experimental design of wet micro sandblasting process. (a) equipment and (b) fixture.

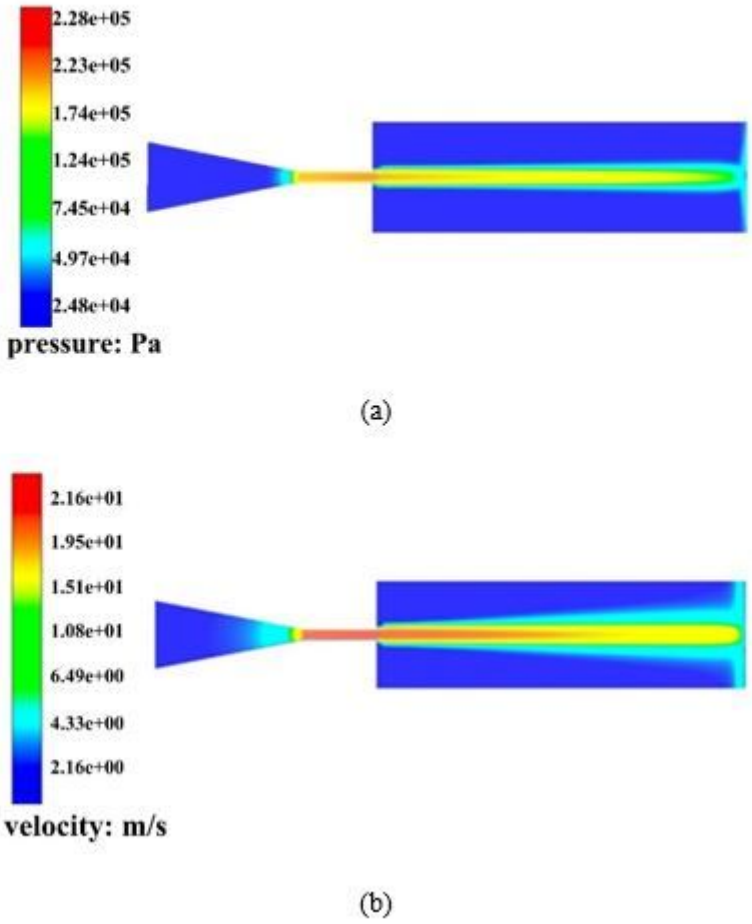

Figure 3

(a) Pressure and (b) velocity cloud map of the flow field at pressure of 0.3 MPa with Al2O3 solid phase.

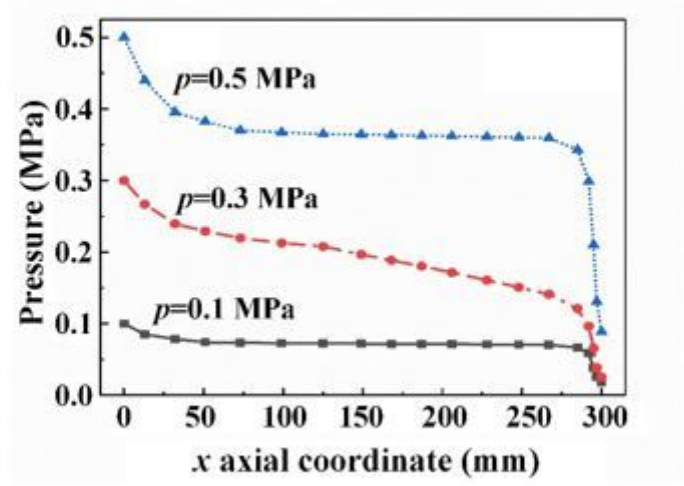

(a)

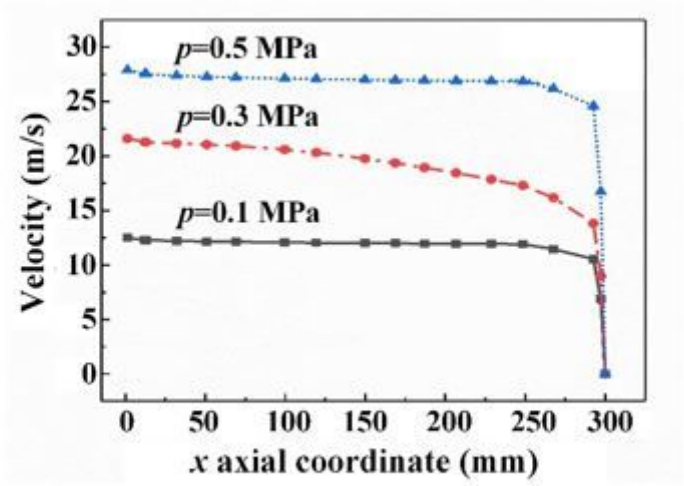

(b)

Figure 4

Variation of (a) pressure and (b) velocity along x axial coordinate (y=0, z=0, solid phase is Al2O3).

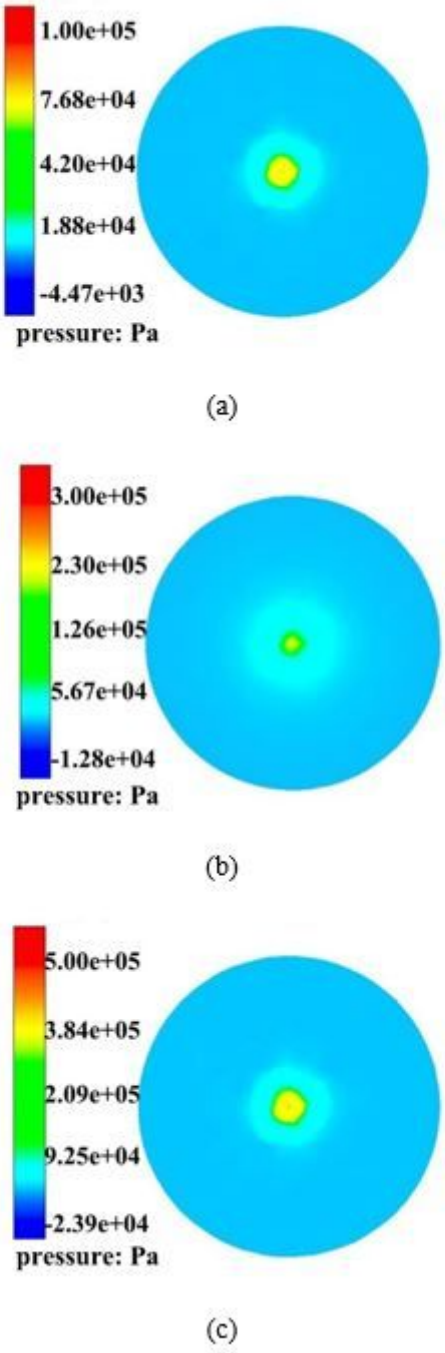

Figure 5

Pressure cloud map of target surface (x=300 mm) at (a) p=0.1 MPa, (b) p=0.3 MPa and (c) p=0.5 MPa.

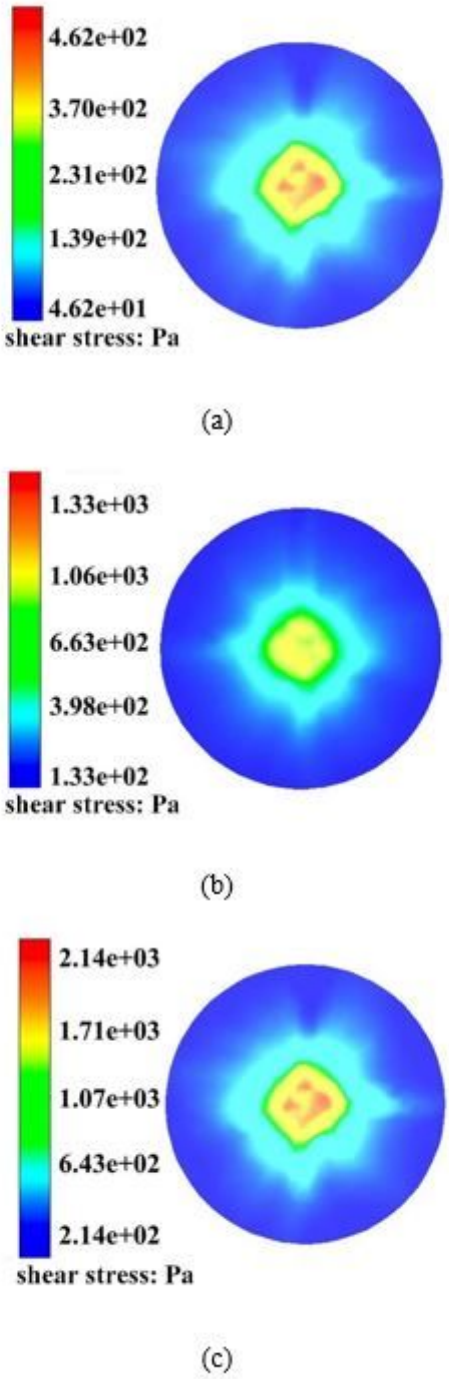

Figure 6

Shear stress cloud map of target surface (x=300 mm) at (a) p=0.1 MPa, (b) p=0.3 MPa and (c) p=0.5 MPa.

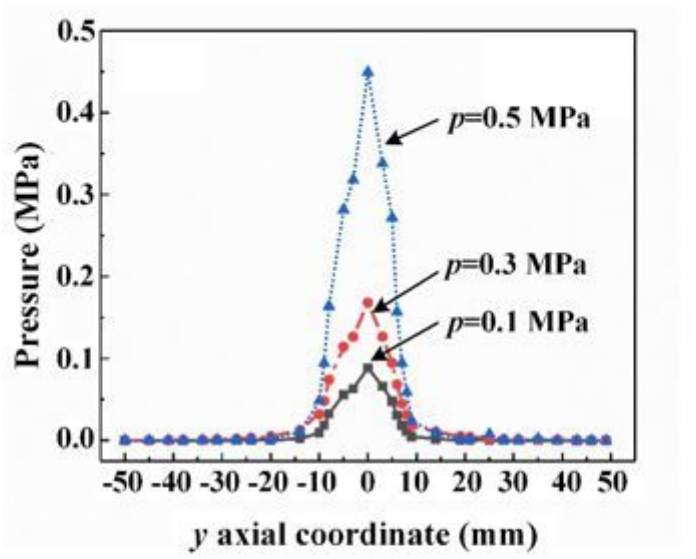

(a)

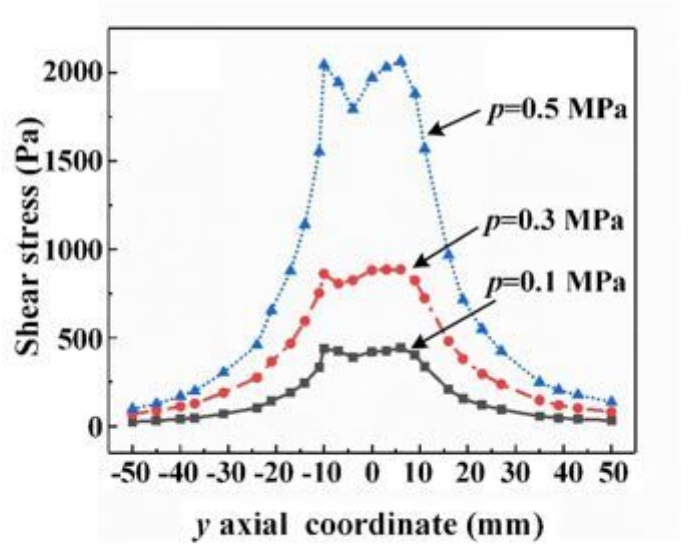

(b)

Figure 7

Variation of (a) pressure and (b) shear stress along y axial coordinate (x=300, z=0, solid phase is Al2O3).

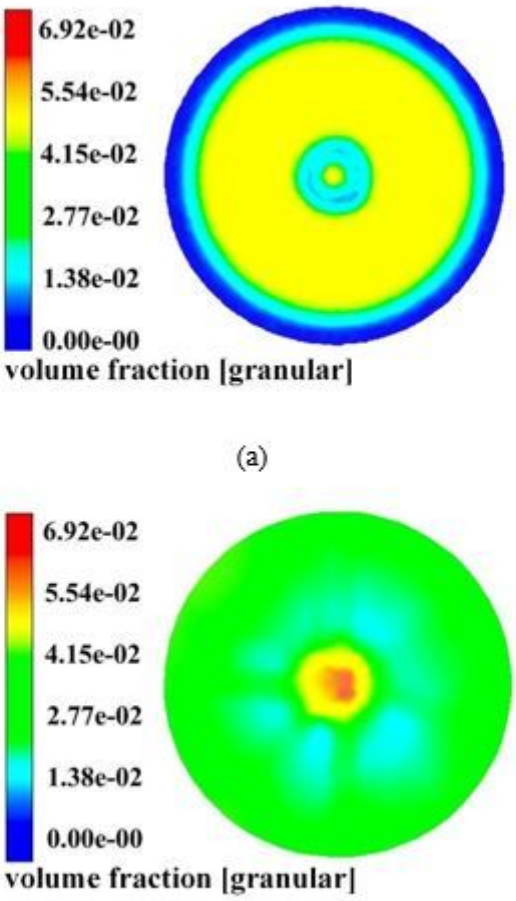

Figure 8

Spray distribution cloud map at (a) x=100 mm and (b) x=300 mm.

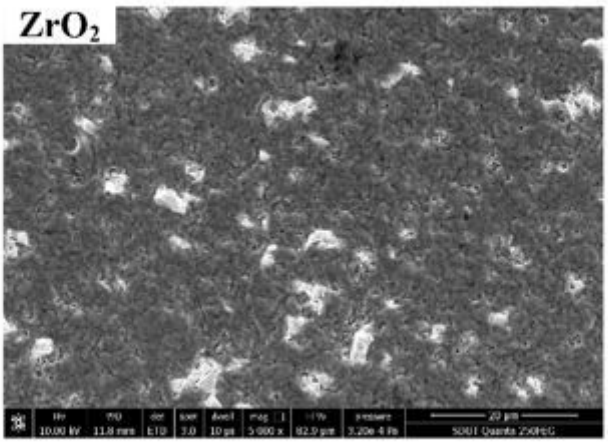

(a)

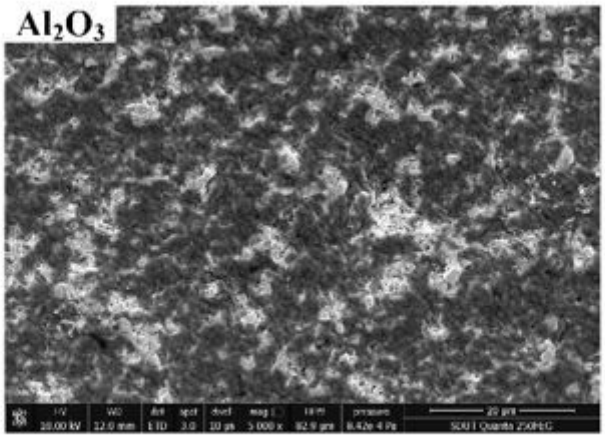

(b)

Figure 9

Effect of abrasive on surface morphology of coated tool at t=5 s and p=0.3 MPa. (a) ZrO2, (b) Al2O3.

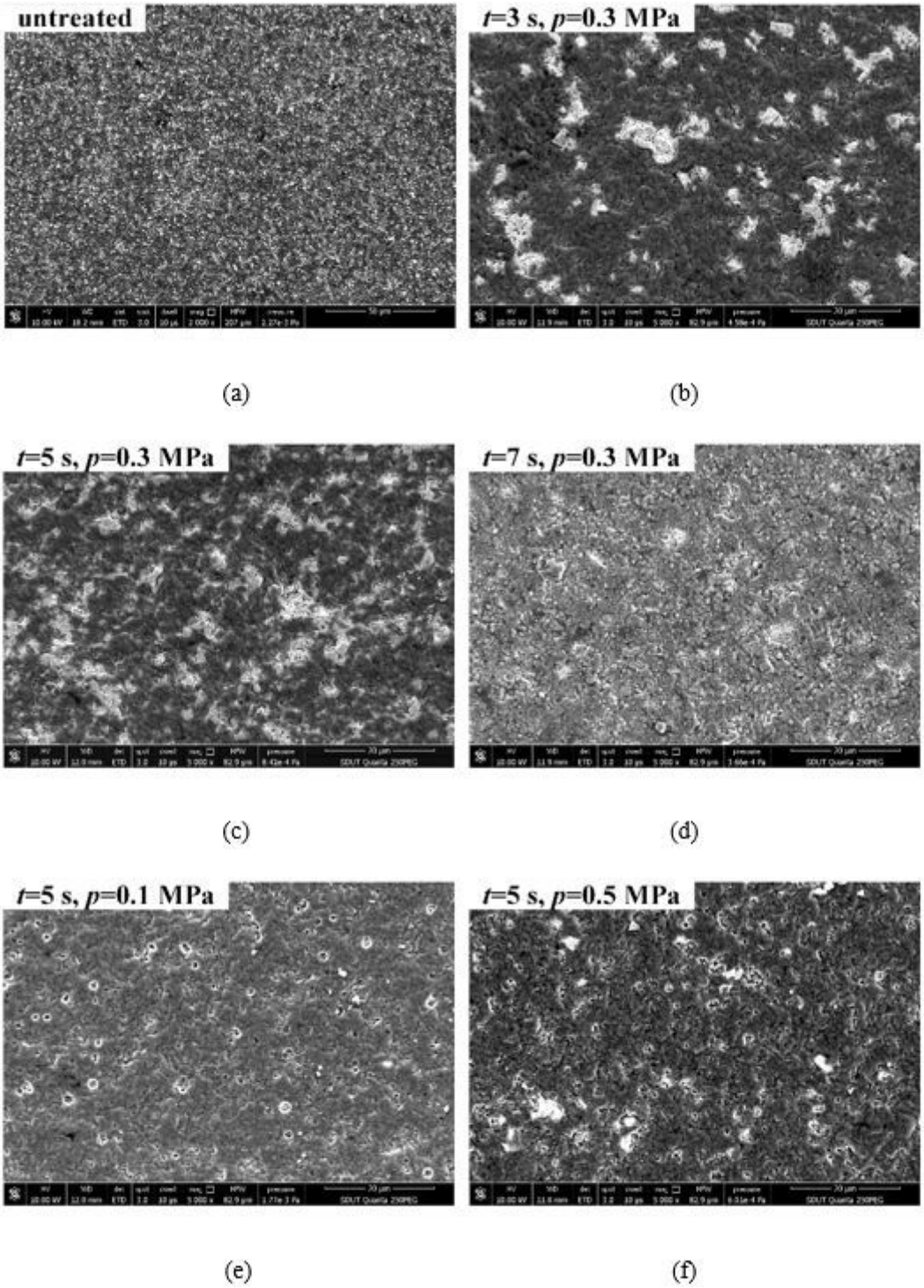

Figure 10

Effect of sandblasting pressure and time on surface morphology of coated tool with abrasive of Al2O3.

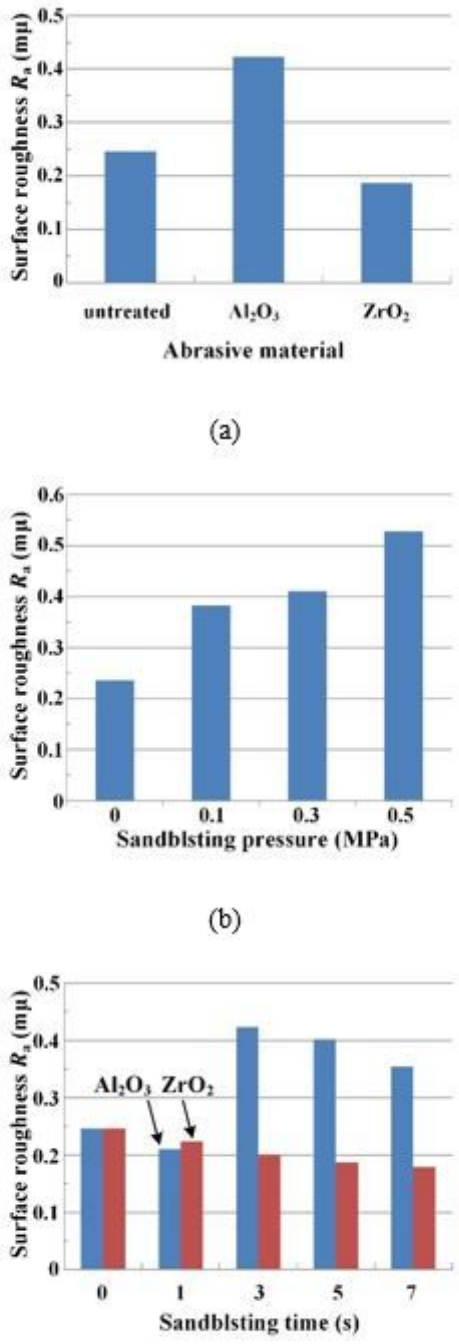

Figure 11

Effect of sandblasting parameters on surface roughness Ra, (a) t=5 s and p=0.3 MPa, (b) Al2O3 and t=5 s, and (c) p=0.3 MPa.

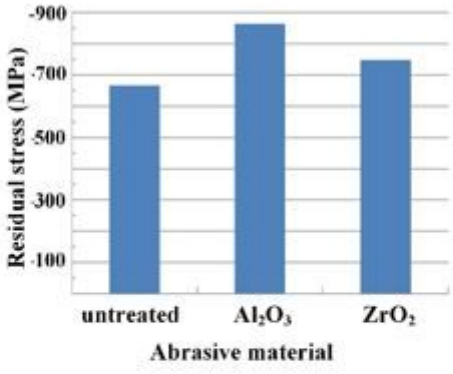

(a)

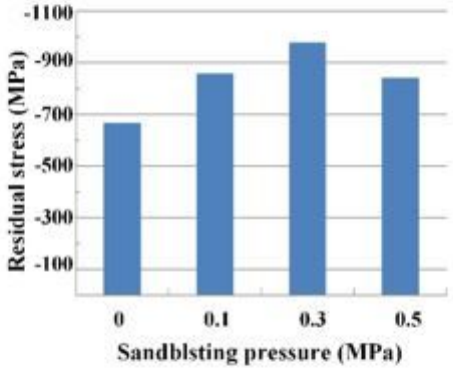

(b)

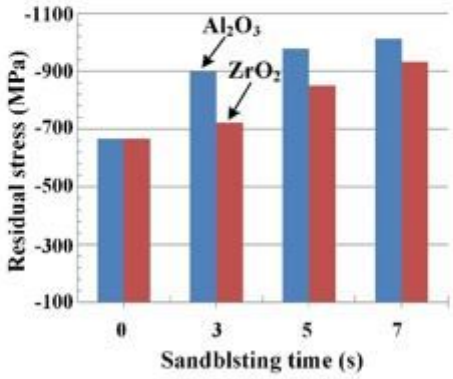

(c)

Figure 12

Effect of sandblasting parameters on residual stress, (a) t=5 s and p=0.3 MPa, (b) Al2O3 and t=5 s, and (c) p=0.3 MPa.